

Diffusion inside living human cells

N. Leijnse¹, J.-H. Jeon², S. Loft⁴, R. Metzler^{3,2}, and L.B. Oddershede^{1,a}

¹ Niels Bohr Institute, University of Copenhagen, Blegdamsvej 17, 2100 Copenhagen Ø, Denmark

² Department of Physics, Tampere University of Technology, 33101 Tampere, Finland

³ Institute for Physics and Astronomy, University of Potsdam, 14476 Potsdam-Golm, Germany

⁴ Institute for Public Health, University of Copenhagen, Øster Farimagsgade 5, 1014 Copenhagen K, Denmark

Received 23 December 2011 / Received in final form 22 February 2012

Published online 17 April 2012

Abstract. Naturally occurring lipid granules diffuse in the cytoplasm and can be used as tracers to map out the viscoelastic landscape inside living cells. Using optical trapping and single particle tracking we found that lipid granules exhibit anomalous diffusion inside human umbilical vein endothelial cells. For these cells the exact diffusional pattern of a particular granule depends on the physiological state of the cell and on the localization of the granule within the cytoplasm. Granules located close to the actin rich periphery of the cell move less than those located towards to the center of the cell or within the nucleus. Also, granules in cells which are stressed by intense laser illumination or which have attached to a surface for a long period of time move in a more restricted fashion than those within healthy cells. For granules diffusing in healthy cells, in regions away from the cell periphery, occurrences of weak ergodicity breaking are observed, similar to the recent observations inside living fission yeast cells [1].

1 Introduction

Diffusion is probably the most important transportation mechanism inside a living cell. Diffusion is highly efficient on length and time scales relevant within the cytoplasm and, as opposed to transport mediated by molecular motors, it only requires thermal energy. The diffusing cargo can be any of the substances present inside the cell, e.g., proteins, lipids, biopolymers, or viral capsids. Not only for a fundamental understanding, but also to take advantage of cellular behavior in the treatment of diseases it is important to uncover the diffusional processes inside a living cell. For instance, to perform a targeted drug delivery one method is to deliver the drug in a nanometer-scale functionalized carrier small enough to diffuse through the target cell membranes and eventually reach a certain cellular compartment [2]. Many viruses, e.g., Hepatitis C virus, use endocytosis for their entry into a host cell [3] and diffuse

^a e-mail: oddershede@nbi.dk

along particular pathways inside the cell. Understanding diffusion processes inside the crowded networks in human cells is thus a major key for cellular delivering of nano-sized functional drugs and for elucidating the pathways in viral infections.

Mathematically, the diffusion process can be described as a scaling of the mean squared displacement, $\langle \mathbf{r}^2(t) \rangle$:

$$\langle \mathbf{r}^2(t) \rangle \propto t^\alpha, \quad (1)$$

where t is time and α the scaling exponent. For $0 < \alpha < 1$ we observe subdiffusion, for $\alpha = 1$ normal Brownian motion, while for $\alpha > 1$ the process becomes superdiffusive [4,5]. Indeed, subdiffusion of proteins, biopolymers or lipid granules has been observed inside living cells, for example inside *Escherichia coli* [6,7], fission yeast *Schizosaccharomyces pombe* (*S. pombe*) cells [1,8,9], and epithelial cells [10]. Other structures also show subdiffusive behavior, such as telomeres in the nucleus of mammalian cells [11] and microspheres engulfed by human cells [12]. Subdiffusion is probably beneficial for the cell [6,13] and can be caused by a crowded environment [14–17].

S. pombe has been used as a model system to study the viscoelastic landscape in eucaryotic cells by tracking the motion of naturally occurring lipid granules using single particle tracking microscopy or by optical trapping [1,8,9,18]. Lipid granules are spherically shaped lipid reservoirs about 300–400 nm in diameter, which is comparable to the size of, e.g., endocytosed vesicles and poxviruses [19]. Lipid granules are excellent tracers of *in vivo* diffusion as they are clearly visible and traceable when viewed using bright field microscopy. Additionally, their high refractive index in comparison to the cytoplasm allows them to be optically trapped thus providing a considerably better temporal resolution than image based single particle tracking.

Here, we investigate the viscoelastic properties of the human umbilical vein endothelial cell (HUVEC) cytoplasm using endogenously occurring lipid granules as tracers. This cell type is particularly interesting with respect to drug delivery assays because endothelial cells line all blood vessels, hence, they constitute the first cell type a drug injected into the bloodstream encounters. HUVECs have a softer cell membrane than *S. pombe* and, when cultured, they vary in shape from one cell to another. They ball up in liquid suspension and flatten out on surfaces with a typical diameter of about 20 μm when spread out. The central region of a cell around the nucleus is approximately 10–15 μm high, and the cell flattens out considerably towards its periphery, which contains a densely branched actin-filament network [20]. We tracked the diffusional motion of lipid granules using optical tweezers and single particle tracking microscopy both in healthy and in stressed HUVEC cells and in different locations within the cell. The diffusive processes of individual granules proved to be highly dependent both on the physiological condition of the cell and on the exact location of the granule within the cell. Within a single cell co-existence of ergodic and non-ergodic processes was found in different cell regions.

2 Methods

2.1 Analysis

The time series of the positions visited by the lipid granules in the imaging plane (x, y) were analyzed in terms of the time averaged mean squared displacement (TA MSD), $\overline{\delta^2(\Delta, T)}$, as function of the lag time, Δ :

$$\overline{\delta^2(\Delta, T)} = \frac{1}{T - \Delta} \int_0^{T-\Delta} [\mathbf{r}(t + \Delta) - \mathbf{r}(t)]^2 dt, \quad (2)$$

where T is the total measurement time [21–25]. \mathbf{r} denotes the two dimensional vector (x, y) where the x and y coordinate axes were random with respect to cell orientation (in contrast to *S. pombe* cells HUVECs do not have a natural axis, they appear symmetric in the observation plane).

Ensemble averages of the mean squared displacements (EA MSDs) are calculated from the positional time series as

$$\langle \mathbf{r}^2(t) \rangle = \frac{1}{N} \sum_{i=1}^N [\mathbf{r}_i(t) - \mathbf{r}_i(0)]^2, \quad (3)$$

where N is the total number of measurements.

2.2 Optical tweezers tracking

Optical tweezers were used to track the position of the lipid granules with a time resolution of 4.5×10^{-5} seconds. The optical trap was implemented in an inverted microscope (Leica DMIRBE) where the laser beam (Nd : YVO₄ (5W Spectra Physics BL106C, $\lambda = 1064$ nm, TEM_∞)) was tightly focused by an oil immersion objective (Leica, HCX, PL, APO, 100x, NA = 1.4, oil). The scattered laser light passing the sample was collected by a condenser (Leica, P1 1.40 oil S1) and focused onto a quadrant photodiode (S5981, Hamamatsu). Data was acquired by a fast data acquisition card (NI PCI-6040E) at a sampling frequency of 22kHz and processed by custom made LabVIEW programs (LabVIEW 2010, National Instruments). The laser power was kept relatively low (120 mW at the exit of the laser of which $\sim 20\%$, 24 mW, reaches the sample) with a typical measurement time of 3 seconds thus making it highly unlikely that the cells would be physiologically affected by the laser light [26]. The temperature increase related to absorption of the laser light is expected to be well below 1°C [27, 28]. Just before data acquisition started the laser was focused on the granule such that the granule was approximately in the center of the weak harmonic potential exerted by the optical trap [29]. The voltage output from the photodiode is linearly related to the distance travelled by the granule, however, in order to convert the voltage output from the photodiode to metric distance knowledge about the viscosity of the medium surrounding the granule and its exact shape would be required. As these parameters are unknown the mean squared displacement data for optical trapping tracking are given in arbitrary units (as was also done in Ref. [1]). The three orthogonal translational directions are uncorrelated and all measurements were done in two dimensions.

In some experiments we deliberately stressed the cells. This was done by focusing the laser at the nucleus of the cell and illuminating the nucleus using a relatively high laser intensity (1900–2900 mW at the exit of the laser) for 5 minutes. Immediately thereafter laser power was decreased and the laser focused on a granule for tracking its position as described above.

2.3 Single particle tracking

In order to track the position of the granules at longer times than possible by optical tweezers tracking we imaged the granules by bright field microscopy and analyzed the pictures by single particle tracking routines. The sample was placed on a Leica microscope with an oil immersion objective (HCX, PL, APO, 100x, NA = 1.4, oil) and images were acquired using an AVT Pike F100B camera (Allied Vision Technologies) using SmartView (Allied Vision Technologies) acquisition software. 225 frames per second were recorded during a total measurement time of 40 seconds. Particle tracking was done using a Matlab (MATLAB R2010a, MathWorks) algorithm [30].

2.4 Preparation of HUVEC samples

HUVECs (Cytotech, Denmark) were cultured in T25 cell culture flasks (Nunclon Δ Surface, Nunc) at 37°C in a 5% CO₂ incubator. They were passaged by washing with PBS buffer, detaching with 0.5% Trypsin EDTA (Gibco) and diluting with endothelial cell growth medium (Endothelial cell growth medium kit, Cell Applications Inc.) before they were seeded in new flasks. All cells used were in passage 3 to 8.

Clean coverslips (24 × 50 mm, #1.5, Menzel-Gläser) were coated with collagen IV (Human placenta Collagen IV, Sigma) and placed in 60 mm petri dishes. HUVEC cells suspended in endothelial cell growth medium were poured into the petri dishes and left in the incubator (typically for 1-2 days) in order to allow the cells to adhere to the coverslips. The density of cells was not high enough to reach a confluent monolayer, some cells were isolated, however, some cells did have contact to other cells. A coverslip was taken out of the petri dish and a perfusion chamber was created by adding two stripes of vacuum grease on this coverslip and placing a clean coverslip (18x18mm, #1, Menzel-Gläser) on top. The chamber was washed and filled with endothelial cell growth medium and sealed off airtight with vacuum grease. Experiments were conducted on a temperature controlled microscope stage (~37°C).

3 Results and discussion

In our experiments we investigated healthy cells: these cells spread out on the collagen surface, have well defined edges, and a clearly distinctive nucleus in their center region. By contrast, compromised cells tend to ‘ball up’ or have an irregular appearance suggesting early stages of cell death. A typical image of the healthy HUVEC cells investigated is shown in Fig. 1(a). The borders of the cell and its nucleus are indicated by white lines. Inside the nucleus the nucleolar region is also distinctive. The visual appearance of a lipid granule depends on its position with respect to the focus of the objective. If the granules are slightly above the focus plane they will appear bright, as do most granules in Fig. 1(a).

3.1 Short time scales

Healthy cells. In Fig. 1(a) the images of 10 granules have been overlaid with white circles and crosses in different colors. The TA MSD trajectories for these 10 granules have been depicted in Fig. 1(b). On time scales between 0.05 and 0.5 ms the scaling behavior of the trajectories of granules inside the nucleus (blue) and in the middle of the cell (magenta) obey $\overline{\delta^2} \sim \Delta$. The TA MSD trajectories of granules on the edge of a cell (green) have a smaller scaling exponent as $\overline{\delta^2} \sim \Delta^{0.75}$ on these short time scales. At around 3 ms, all trajectories show a turnover to a smaller slope of around 0.2 due to the confinement of the optical tweezers [1].

The tendency apparent from the individual TA MSD traces (Fig. 1(b)) is even more clear when one considers the average of all individually measured TA MSD traces (223 granules) as shown in Fig. 2(a). Clearly, the scaling behavior depends on the cellular location of the granules with a scaling exponent close to 1 at short times for granules located in the nucleus or close to the nucleus. The TA MSD scaling exponent for granules located at the cellular periphery is closer to 0.75, a sign of conventional subdiffusion. On the contrary, the EA MSD (defined in Eq. (3)) of the trajectories of all 223 granules have a scaling exponent of 0.75, this being independent of their location within the cell. Hence, TA MSD averages and EA MSD differ for granules close to or inside the nucleus on short time scales. This

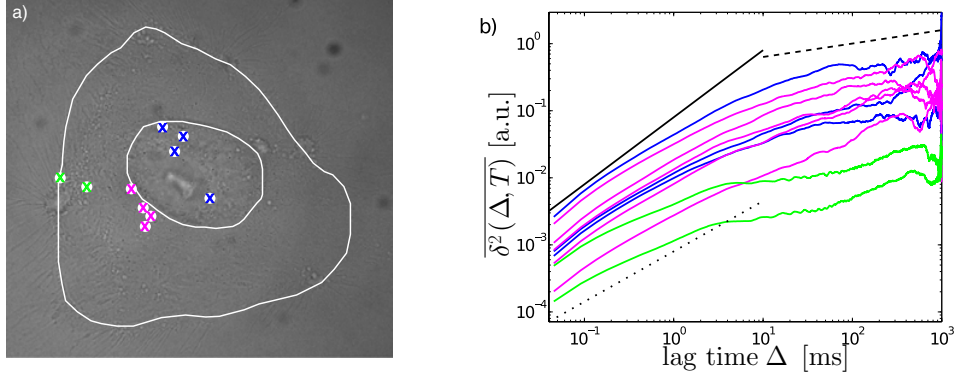


Fig. 1. Diffusion of individual lipid granules. a) Picture of a typical HUVEC. The borders of the cell and its nucleus are enhanced by a white line. Approximate positions of 10 tracked granules are marked and color coded accordingly to their locations (blue: in nucleus, magenta: close to nucleus, green: at the cell periphery). b) TA MSD trajectories, $\overline{\delta^2}$, for the 10 granules marked in a). Color code matches a). The black lines have slopes of 1 (full), 0.75 (dotted) and 0.2 (dashed).

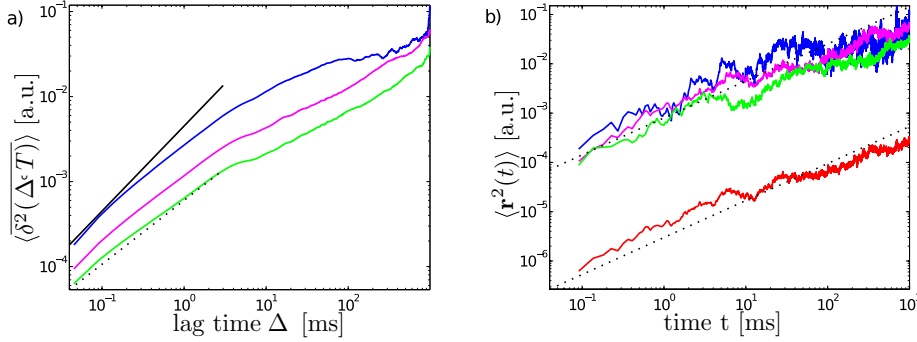


Fig. 2. Averages of granules trajectories in healthy cells. a) Averages of TA MSD, $\langle \overline{\delta^2} \rangle$, from granules at different locations (blue: in nucleus $n = 35$, magenta: close to nucleus $n = 144$, green: cell periphery $n = 44$). Black lines have slopes of 1 (full line) and 0.75 (dotted line). b) EA MSD $\langle \mathbf{r}^2 \rangle$ for granules at different locations, color coding of blue, magenta, and green traces as in a). The red trace is an average of all 223 trajectories and has been artificially shifted downwards for visibility. Both dotted lines have a slope of 0.75.

implies the presence of so-called weak ergodicity breaking. For granules at the cellular periphery $\overline{\delta^2} \approx \langle \mathbf{r}^2 \rangle \sim \Delta^{0.75}$. Hence, there is no sign of ergodicity breaking for granules located close to the cellular periphery. Recently, similar co-existence of ergodic and non-ergodic processes has also been shown within plasma membranes [31]. For the fission yeast *S. pombe* weak ergodicity breaking was consistently found throughout the entire cytoplasm [1]. However, there are major differences between the cytoplasm of *S. pombe* and HUVECs, also, *S. pombe* cells are cylindrically shaped ($\sim 4 \mu\text{m} \times 12 \mu\text{m}$) while HUVECs have a “fried egg” appearance: the cell is highest at its nucleus and flattens out in all directions towards its shallow periphery. The diameter of a HUVEC is $\sim 20 \mu\text{m}$ and its height at the nucleus is $\sim 10\text{--}15 \mu\text{m}$. The exact height of the HUVEC’s periphery is unknown, however, based on confocal images in [32] it is probably on the order of $1\text{--}2 \mu\text{m}$. Possibly, the differences of TA MSD scaling properties are due to the fact that actin is abundantly present at the

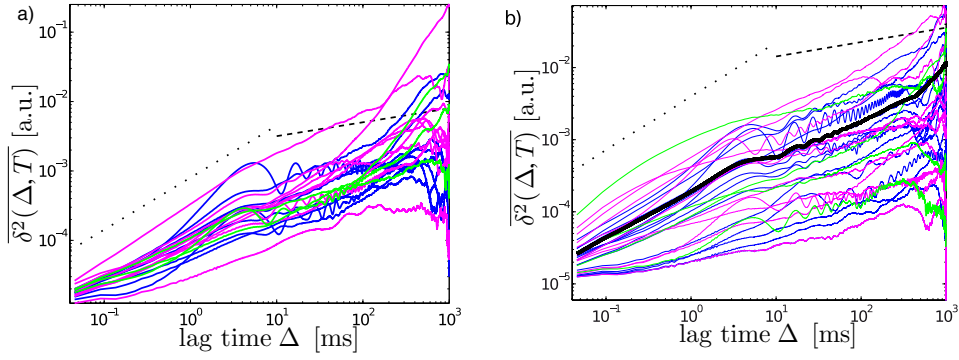


Fig. 3. TA MSD for irradiated cells or cells which firmly attached during 6 days to the coverslip. a) TA MSD, $\overline{\delta^2}$, for 20 granules in cells with highly irradiated nucleus. The color code signifies the granule's location (blue: in nucleus, magenta: close to nucleus, green: cell periphery). Black lines have slopes of 0.75 (dotted) and 0.2 (dashed). b) TA MSD, $\overline{\delta^2}$, for 30 granules in cells which were allowed to firmly attach to the collagen coated coverslip during 6 days. Color code as in a). The thick black trajectory is the average of all shown TA MSD trajectories. Straight black lines have slopes of 0.75 (dotted), and 0.2 (dashed).

periphery of the cell thus making the local environment more elastic (less viscous) than the cytoplasm closer to the central region. Also, as the cell is rather shallow towards the edges the proximity of the membranes may result in a larger friction on the granules, thus restricting their motion [33,34]. Correlations between diffusional properties of lipid granules and their locations within living human cells have been earlier reported [10], albeit, at timescales larger than here described.

Stressed cells. When the cells were stressed by 5 minutes continuous irradiation of their nucleus at high laser power they changed visual appearance and became 'balled up', a sign of physiological stress. It is unknown exactly how the laser light affects the nucleus, however, it is known that the integrated amount of deposited energy has an effect on protein regulation and expression. Also, it is possible at these high laser powers that the temperature locally increases maybe tens of degrees thus possibly affecting cellular processes. Immediately after stressing the cells normal measurements of TA MSD were performed, these are shown in Fig. 3(a). These TA MSD trajectories appear distinctly different from those originating from healthy cells (Fig. 1(b)); the scaling exponents characterizing the TA MSD trajectories of granules inside stressed cells scale with exponents of 0.75 or smaller for short times, at later times there is a turnover to an exponent of ~ 0.2 . There is no clear dependence on localization. Hence, exerting stress on the cell gives rise to different scaling behavior of the TA MSD trajectories.

The visual appearance of HUVECs which had attached for 6 days on a collagen coated surface was similar to the healthy cells which only had attached for 1-2 days. TA MSD trajectories for granules in cells which attached for 6 days are shown in Fig. 3(b). All trajectories scale with exponents < 1 and a turnover to a lower exponent is present for times > 4 ms. There is no clear localization dependence. If a cell has had an extensive time to adhere and spread out onto a surface, its cytoskeleton has remodeled and actin polymerized in all regions [35] of the cell. Thus, the observation of relatively low TA MSD scaling exponents (often around 0.75) for all regions of a strongly attached cell is consistent with our observation (Figs. 1(b) and 2(a)) that the TA MSD trajectories for granules in actin rich regions at the cellular periphery scale with $\Delta^{0.75}$.

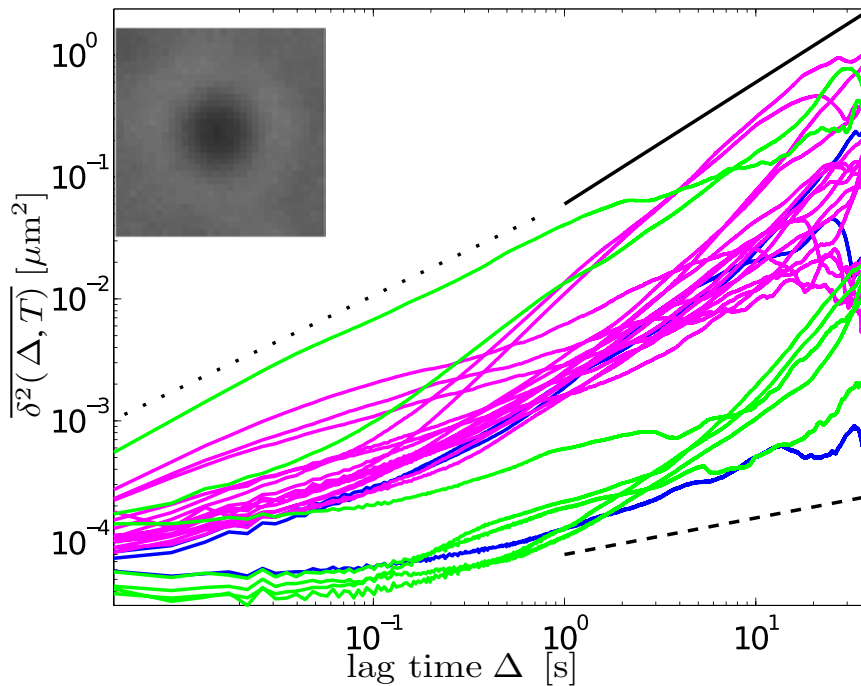


Fig. 4. Single particle tracking TA MSD trajectories of granules. The color coding signifies the location of the granule (blue: in nucleus, magenta: close to nucleus, green: cell periphery). Black lines have slopes of 1 (full), 0.75 (dotted), and 0.3 (dashed). The inset shows a typical picture of a tracked granule.

Oscillations. In some of the TA MSD trajectories for individual granules shown in Figs. 3(a), and 3(b) clear oscillations are present. These appear to start, or have a pronounced bump, around 4 ms and fade out at longer times. The onset time approximately coincides with the onset of the confinement by the optical trapping potential. Interestingly, such oscillations were consistently present in the TA MSD curves for *S. pombe* [1] and are analogous to subdiffusion in an underdamped medium. The oscillations are not as consistently present in every single TA MSD curve for granules in HU-VECs as was the case for granules in *S. pombe*. In order to check that the oscillations were not an artifact from the equipment we changed lasers, microscope, photodiodes, measurement height, etc. However, the oscillations prevailed in the trajectories and could not be contributed to instrumental artifacts. We defined an oscillation as a pronounced bump around 4 ms and 4 consecutive distinctive oscillations. With this definition we went through all trajectories and analyzed which trajectories were most likely to have oscillations: More stressed cells (40% of 20 granules) had oscillations in the TA MSD trajectories than did healthy cells (34% of 223 granules). And for the stressed cells, oscillations happened more frequently for granules located in the nucleus of the cell (63% of 8 granules) than in the remaining cytoplasm (25% of 12 granules).

3.2 Longer time scales

At longer timescales the trajectories of the granules were tracked by video microscopy, the inset in Fig. 4 shows a picture of a tracked granules, the objective is zoomed in

and focused slightly below the granules such that it appears dark with respect to its background. The video based method has the advantage that it does not exert a confining potential, however, the temporal resolution is not as low as with the optical trap. Figure 4 shows the TA MSD trajectories obtained by single particle tracking. Initially all slopes are around 0.75 (or below), consistent with the short time data. At around 1 s the trajectories differentiate substantially, some trajectories show a confinement ($\alpha = 0$), some show normal diffusion ($\alpha = 1$), others super diffusion ($\alpha > 1$). This is reasonable as the biological processes, for instance, transport of lipid granules by molecular motors or remodeling of the cytoskeleton, become detectable at timescales of seconds or longer. Granules at the periphery of the cell move somewhat less than granules in the inner regions. At the periphery, granules are probably restricted in their mobility due to the dense network of cortical actin, it is a general property of polymer networks that they restrict mobility [20, 33, 34]. In addition, the shallowness of the cell in this region probably restricts the mobility. For a granule embedded in a semiflexible polymer network (with mesh size of the order 100 nm to 1 μm) or for a granule confined between larger cell organelles, $\overline{\delta^2}$ would show a plateau for longer lag times, Δ , around 1–10 s [33]. This is visible for few of the trajectories between 1 and 10 s.

4 Conclusion

Lipid granules exhibit anomalous diffusion inside human umbilical vein endothelial cells (HUVECs). By comparing time averaged mean squared displacements of individual trajectories to the corresponding ensemble averaged mean squared displacement trajectories we showed the presence of weak ergodicity breaking at short times for granules located in the nucleus or close to the nucleus in healthy HUVECs. We did not observe ergodicity breaking for granules located towards the periphery of the cell, for granules located in stressed cells, or for granules in cells which attached firmly to a collagen coated coverslip for an extended period of time. The fact that granules appeared to be moving less freely close to the cellular periphery or in cells which were allowed to adhere for six days is probably related to the presence of a dense cortical actin network at the cellular periphery and a dense microtubule and actin network throughout the entire cytoplasm of cells which were allowed to adhere for an extended period of time. Hence, within a single healthy HUVEC we observed a coexistence of ergodic and non-ergodic processes, as also observed within the plasma membrane [31].

The observation that the trajectories of lipid granules inside HUVECs depend on the location of the granules within the cytoplasm as well as on the physiological state of the cell contrasts observations from the fission yeast *S. pombe*. Inside *S. pombe* weak ergodicity breaking was consistently observed at short time scales for granules located throughout the cytoplasm [1]. Hence, compared to fission yeast cells, human cells appear to have a more complex, regional structuring of the cytoplasm, inducing different phenomenology of the diffusion behavior of large, inert tracers such as lipid granules. When investigating diffusional processes inside living human cells, for instance in relation to drug delivery or viral infections, special attention should be paid to the physiological state of the cell.

Though we believe that the regular oscillations present at timescales around 10 ms both in the optical tweezers data and in the single particle tracking data (which were also observed in the motion of lipid granules inside *S. pombe* cells [1]) are connected to the fact that the particles perform subdiffusion in an underdamped medium, it still remains an open problem to fully understand the origin of these oscillations.

Also, it still remains a theoretical challenge to pinpoint the true nature of the anomalous diffusive process inside a living cell, it may be a continuous time random walk, a fractional Brownian motion, diffusion on a fractal, or maybe a combination of these.

We acknowledge important advice from and discussions with P.M. Bendix, H. Klingberg, S.N.S. Reihani, N.S. Rossen, and M. Roursgaard. NL, SL, and LBO acknowledge funding from the Lundbeck Foundation 'Center for Biomembranes in Nanomedicine' and from the University of Copenhagen Excellence program. JHJ and RM acknowledge funding from the Academy of Finland (FiDiPro scheme).

References

1. J.H. Jeon, V. Tejedor, S. Burov, E. Barkai, C. Selhuber-Unkel, K. Berg-Sørensen, L.B. Oddershede, R. Metzler, *Phys. Rev. Lett.* **106**, 048103 (2011)
2. L. Rajendran, H.J. Knolker, K. Simons, *Nat. Rev. Drug. Discov.* **9**, 29 (2010)
3. D. Moradpour, F. Penin, C.M. Rice, *Nature Microbiol.* **5**, 453 (2007)
4. R. Metzler, J. Klafter, *Physics Reports* **339**, 1 (2000)
5. R. Metzler, J. Klafter, *J. Phys. A: Math. General* **37**, R161 (2004)
6. I. Golding, E. Cox, *Phys. Rev. Lett.* **96**, 098102 (2006)
7. S.C. Weber, A.J. Spakowitz, J.A. Theriot, *Phys. Rev. Lett.* **104**, 238102 (2010)
8. I.M. Tolić-Nørrelykke, E.L. Munteanu, G. Thon, L.B. Oddershede, K. Berg-Sørensen, *Phys. Rev. Lett.* **93**, 078102 (2004)
9. C. Selhuber-Unkel, P. Yde, K. Berg-Sørensen, L.B. Oddershede, *Phys. Biol.* **6**, 025015 (2009)
10. S. Yamada, D. Wirtz, S.C. Kuo, *Biophys. J.* **78**, 1736 (2000)
11. I. Bronstein, Y. Israel, E. Kepten, S. Mai, Y. Shav-Tal, E. Barkai, Y. Garini, *Phys. Rev. Lett.* **103**, 018102 (2009)
12. A. Caspi, R. Granek, M. Elbaum, *Phys. Rev. E* **66**, 011916 (2002)
13. G. Guigas, M. Weiss, *Biophys. J.* **94**, 90 (2008)
14. R.J. Ellis, A.P. Minton, *Nature* **425**, 27 (2003)
15. S.R. McGuffee, A.H. Elcock, *PLoS Comput Biol.* **6**, e1000694 (2010)
16. M.J. Saxton, K. Jacobson, *Annual Rev. Biophys. Biomolec. Struct.* **26**, 373 (1997)
17. G. Seisenberger, M.U. Ried, T. Endreß, H. Büning, M. Hallek, C. Bräuchle, *Science* **294**, 1929 (2001)
18. V. Tejedor, O. Benichou, R. Voituriez, R. Jungmann, F. Simmel, C. Selhuber-Unkel, L. Oddershede, R. Metzler, *Biophys. J.* **98**, 1364 (2010)
19. J. Mercer, M. Schelhaas, A. Helenius, *Annu. Rev. Biochem.* **79**, 803 (2010)
20. D.A. Fletcher, R.D. Mullins, *Nature* **463**, 485 (2010)
21. Y. He, S. Burov, R. Metzler, E. Barkai, *Phys. Rev. Lett.* **101**, 058101 (2008)
22. S. Burov, R. Metzler, E. Barkai, *Proc. National Acad. Sci.* **107**, 13228 (2010)
23. S. Burov, J.H. Jeon, R. Metzler, E. Barkai, *Phys. Chem. Chem. Phys.* **13**, 1800 (2011)
24. A. Lubelski, I.M. Sokolov, J. Klafter, *Phys. Rev. Lett.* **100**, 250602 (2008)
25. T. Neusius, I.M. Sokolov, J.C. Smith, *Phys. Rev. E* **80**, 011109 (2009)
26. M. Rasmussen, L. Oddershede, H. Siegmundfeldt, *Appl. Environm. Microbiol.* **74**, 2441 (2008)
27. E. Peterman, F. Gittes, C. Schmidt, *Biophys. J.* **84**, 1308 (2003)
28. P. Bendix, S. Reihani, L. Oddershede, *ACS Nano* **4**, 2256 (2010)
29. A.C. Richardson, S.N.S. Reihani, L.B. Oddershede, *Opt. Express* **16**, 15709 (2008)
30. S.S. Rogers, T.A. Waigh, X. Zhao, J.R. Lu, *Phys. Biol.* **4**, 220 (2007)

31. A.V. Weigel, B. Simon, M.M. Tamkun, D. Krapf, Proc. National Acad. Sci. **108**, 6438 (2011)
32. N. Rossen, A. Hansen, C. Selhuber-Unkel, L. Oddershede, PLoS ONE **6**, e25196 (2011)
33. F. Gittes, F.C. Mackintosh, Phys. Rev. E **58**, R1241 (1998)
34. I.Y. Wong, M.L. Gardel, D.R. Reichman, E.R. Weeks, M.T. Valentine, A.R. Bausch, D.A. Weitz, Phys. Rev. Lett. **92**, 178101 (2004)
35. J.L. McGrath, Current Biol. **17**, R357 (2007)